

Magneto-transport in impurity-doped few-layer graphene spin valve

Kai-He Ding¹, Zhen-Gang Zhu², Zhen-Hua Zhang¹, and Jamal Berakdar²

¹*Department of Physics and Electronic Science, Changsha University of Science and Technology, Changsha, 410076, China*

²*Institut für Physik Martin-Luther-Universität Halle-Wittenberg Nanotechnikum-Weinberg, Heinrich-Damerow-Strasse 4 D - 06120 Halle (Saale), Germany*

Using Keldysh nonequilibrium Green's function method we study the spin-dependent transport through impurity-doped few layer graphene sandwiched between two magnetic leads with an arbitrary mutual orientations of the magnetizations. We find for parallel electrodes magnetizations that the differential conductance possesses two resonant peaks as the applied bias increases. These peaks are traced back to a buildup of a magnetic moment on the impurity due to the electrodes spin polarization. For a large mutual angle of the electrodes magnetization directions, the two resonant peaks approach each others and merge into a single peak for antiparallel orientation of the electrodes magnetizations. We point out that the tunneling magnetoresistance (TMR) may change sign for relatively small changes in the values of the polarization parameters. Furthermore, we inspect the behaviour of the differential conductance and TMR upon varying the temperature.

PACS numbers: 85.75.-d, 75.47.-m, 71.55.-i

I. INTRODUCTION

In the past few years much effort was devoted to the investigations, fabrications and utilizations of graphene samples¹⁻⁴ culminating in a series of fascinating findings such as the anomalous quantized Hall effect, the absence of weak localization and the existence of minimal conductivity³. These phenomena underline the remarkable potential of graphene in future advances in nanoscience. Fueled by this development novel graphene-based technological applications and devices are currently envisaged. In this respect, a special attention has been paid to the spin dependent transport in graphene and graphene-ferromagnet heterostructures, as prototypical spintronic device⁵⁻¹⁴. For example, Hill *et al.*⁵ fabricated graphene spin valves and observed a 10% change in the resistance as the electrodes magnetizations switch orientation from a parallel to an antiparallel configuration. Recent experiments on the spin injection in a single layer graphene show a rather long spin-flip relaxation length $\approx 1\mu\text{m}$ at room temperature⁶. The spin injection into a graphene thin film has been successfully demonstrated by using nonlocal magnetoresistance measurements⁶⁻⁸. Wang *et al.*⁹ measured the magnetoresistance of mesoscopic graphite spin-valve devices and observed a cusplike feature of the magnetoresistance versus the applied bias. Ding *et al.*¹⁰ studied theoretically the spin-dependent transport through the graphene spin valve device, and pointed out that a pronounced cusplike feature at zero bias is due to the result of a subtle combined effect of graphene and the conventional spin-valve properties.

Recently, it has been demonstrated¹⁵ that adatoms can be precisely positioned on graphene. Numerous works evidence that the adatoms may create new many-body states in graphene and lead to extraordinary properties such as magnetism¹⁶⁻¹⁹ and Kondo effect²⁰⁻²⁵, which are different from the case of impurities in an ordinary metal. Therefore, the modification of the properties of graphene by the impurity atoms may also influence the magneto-

transport in graphene nanojunctions, an issue which is addressed here. In this work, we study theoretically the spin dependent transport through few layers of graphene in the presence of impurity atoms. The method is based on the standard Keldysh nonequilibrium Green's function approach, as described in^{26,27}. We find that if the electrodes spin polarization vectors are parallel, the applied bias dependence of the differential conductance exhibits two resonant peaks signaling the formation of the impurity magnetic moment due to the electrodes magnetization. With increasing the mutual angle θ of the electrodes spin polarization vectors the two peaks develop gradually into a single peak at $\theta = \pi$. Thus the electrodes magnetization orientations may be used to switch on and off the magnetism of the impurity atoms. We also investigate the dependence of the tunnel-magnetoresistance on θ , on the temperature, and on the spin polarization degrees of the electrodes in details.

II. SINGLE LAYER GRAPHENE

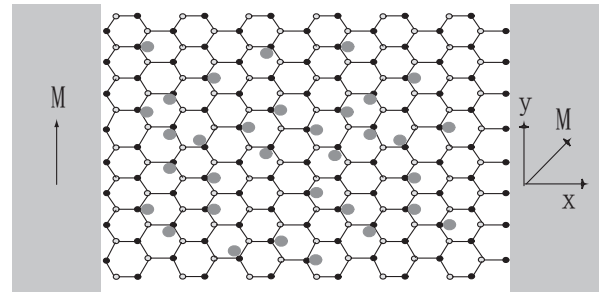


FIG. 1. A schematic illustration of the system considered in this work. A nanotunnel junction made of one or few layers of graphene with impurity atoms is connected to two magnetic leads. The magnetic moments of the leads are aligned by a relative angle θ , and the coupling matrix between α ($\alpha = L, R$) electrode and graphene is $T_{k\alpha}$.

We consider a monolayer graphene sandwiched between two ferromagnetic electrodes. Some impurity atoms are absorbed on the top of carbon atoms in the graphene sheet, as shown in Fig.1. The moment \mathbf{M}_L of the left electrode is assumed to align along the y direction, while the moment \mathbf{M}_R of the right electrode deviates from the y direction by a relative angle θ . A bias voltage V is applied between the left and the right electrodes. The electric current flows in the x direction. The Hamiltonian of this system reads

$$H = H_L + H_R + H_G + H_T + H_i + H_f. \quad (1)$$

Here, $H_L(H_R)$ describes the left(right) electrode:

$$H_L = \sum_{\mathbf{k}, \sigma} \varepsilon_{\mathbf{k}L\sigma} c_{\mathbf{k}L\sigma}^\dagger c_{\mathbf{k}L\sigma} \quad (2)$$

$$H_R = \sum_{\mathbf{k}, \sigma} [\varepsilon_R(\mathbf{k}) - \sigma \mathbf{M}_R \cos \theta] c_{\mathbf{k}R\sigma}^\dagger c_{\mathbf{k}R\sigma} - \mathbf{M}_R \sin \theta c_{\mathbf{k}R\sigma}^\dagger c_{\mathbf{k}R\sigma} \quad (3)$$

where $\varepsilon_{\mathbf{k}\alpha\sigma}$ is the single electron energy, $c_{\mathbf{k}\alpha\sigma}^\dagger(c_{\mathbf{k}\alpha\sigma})$ is the usual creation (annihilation) operator for an electron with the momentum \mathbf{k} and the spin σ in the $\alpha = L, R$ electrode.

The tight-binding Hamiltonian of the electrons in graphene is given by

$$H_G = -t \sum_{\langle i, j \rangle, \sigma} (a_{i, \sigma}^\dagger b_{j, \sigma} + \text{H.c.}), \quad (4)$$

where $a_{i, \sigma}^\dagger(a_{i, \sigma})$ creates (annihilates) an electron with the spin σ on the position \mathbf{R}_i of the sublattice A , $b_{i, \sigma}^\dagger(b_{i, \sigma})$ creates(annihilates) an electron with the spin σ on the position \mathbf{R}_i of the sublattice B , t is the nearest neighbor($\langle i, j \rangle$) hopping energy. In the momentum space Eq.(4) can be rewritten as

$$H_G = \sum_{\mathbf{q}, \sigma} [\phi(\mathbf{q}) a_{\mathbf{q}\sigma}^\dagger b_{\mathbf{q}\sigma} + \phi(\mathbf{q})^* b_{\mathbf{q}\sigma}^\dagger a_{\mathbf{q}\sigma}] \quad (5)$$

where $\phi(\mathbf{q}) = -t \sum_{i=1}^3 e^{i\mathbf{q} \cdot \delta_i}$ with $\delta_1 = \frac{a}{2}(1, \sqrt{3}, 0)$, $\delta_2 = \frac{a}{2}(1, -\sqrt{3}, 0)$, $\delta_3 = a(1, 0, 0)$ (here a is the lattice spacing). The Hamiltonian (5) can be easily diagonalized and one can show $E_\pm(\mathbf{q}) = \pm t |\phi(\mathbf{q})|$, which can be linearized around the \mathbf{K} points of the Brillouin zone and have a dispersion given by

$$E_\pm(\mathbf{q}) = \pm v_F |\mathbf{q}|, \quad (6)$$

where $v_F = 3ta/2$ is the Fermi velocity of an electron. The coupling between the electrodes and graphene is modeled by

$$H_T = \frac{1}{\sqrt{N}} \sum_{\mathbf{k}\alpha\sigma} [T_{\mathbf{k}\alpha\mathbf{q}} c_{\mathbf{k}\alpha\sigma}^\dagger a_{\mathbf{q}\sigma} + \text{H.c.}], \quad (7)$$

where $T_{\mathbf{k}\alpha\mathbf{q}}$ is the coupling matrix between the α electrode and the graphene; N is the number of sites on the sublattice A . Assuming some impurity atoms to be placed on the top of the sublattice A , for the simplicity, we neglect the correlated interaction between the impurities, and express the hybridization with the localized impurity states as

$$H_i = \frac{1}{\sqrt{N}} \sum_{\mathbf{q}l\sigma} V_l (f_{l\sigma}^\dagger a_{\mathbf{q}\sigma} + a_{\mathbf{q}\sigma}^\dagger f_{l\sigma}), \quad (8)$$

where $f_{l\sigma}^\dagger(f_{l\sigma})$ creates(annihilates) an electron with spin σ at the impurity at the site l , and V_l is the random and strength distributions of the hybridization satisfying $\langle V_l V_{l'} \rangle_{dis} = V_0^2 \delta_{ll'}$, where $\langle \dots \rangle_{dis}$ denotes the impurity average^{28,29}.

H_f describes the impurities:

$$H_f = \sum_{l\sigma} \varepsilon_0 f_{l\sigma}^\dagger f_{l\sigma} + U n_{l\uparrow} n_{l\downarrow}, \quad (9)$$

where $n_{l\sigma} = f_{l\sigma}^\dagger f_{l\sigma}$ is the occupation number operator, ε_0 is the single electron energy at the impurity, and the Coulomb interaction is included by a finite U Anderson term. For simplicity, we adopt a mean field approximation to the electronic correlations at the impurity, $U n_{l\uparrow} n_{l\downarrow} \simeq U \sum_{\sigma} \langle n_{l\sigma} \rangle f_{l\sigma}^\dagger f_{l\sigma} - U \langle n_{l\uparrow} \rangle \langle n_{l\downarrow} \rangle$, meaning that the present theory is reliable for temperatures above the Kondo temperatures. The impurity Hamiltonian is rewritten as $H_f = \sum_{\sigma} \varepsilon_{l\sigma} f_{l\sigma}^\dagger f_{l\sigma}$ with $\varepsilon_{l\sigma} = \varepsilon_0 + U \langle n_{l\sigma} \rangle$.

The electric current can be calculated from the time evolution of the occupation number operator of the left electrode.

$$I = e \langle \dot{\mathcal{N}}_L \rangle = \frac{ie}{\hbar} \langle [H, \mathcal{N}_L] \rangle, \quad (10)$$

where $\mathcal{N}_L = \sum_{\mathbf{k}\sigma} c_{\mathbf{k}L\sigma}^\dagger c_{\mathbf{k}L\sigma}$. Using the nonequilibrium Green's function method, Eq.(10) can be further expressed as

$$I = -\frac{ie}{\hbar} \int \frac{d\varepsilon}{2\pi} Tr \{ [\mathcal{G}_a^r(\varepsilon) - \mathcal{G}_a^a(\varepsilon)] f_L(\varepsilon) + \mathcal{G}_a^<(\varepsilon) \} \Gamma_L(\varepsilon), \quad (11)$$

where Tr is the trace in the spin space, $f_\alpha(\varepsilon)$ is Fermi distribution function, $\mathcal{G}_a^r(\varepsilon) = \sum_{\mathbf{q}\mathbf{q}'} \langle G_{\mathbf{q}a, \mathbf{q}'a}^r(\varepsilon) \rangle_{dis}$ and $\mathcal{G}_a^<(\varepsilon) = \sum_{\mathbf{q}\mathbf{q}'} \langle G_{\mathbf{q}a, \mathbf{q}'a}^<(\varepsilon) \rangle_{dis}$ are 2×2 matrices representing the retarded green's function and the lesser Green's function respectively. In the calculation of Eq.(11), we assume that the dominant contributions to tunneling stem from the electrons near Fermi level, and hence assume the linewidth function to be independent of \mathbf{q} . Thus, we have

$$\Gamma_\alpha = \begin{pmatrix} \Gamma_\alpha^\uparrow & 0 \\ 0 & \Gamma_\alpha^\downarrow \end{pmatrix} \quad (12)$$

with $\Gamma_\alpha^\sigma = 2\pi \sum_{\mathbf{k}} T_{\mathbf{k}\alpha\mathbf{q}}^* T_{\mathbf{k}\alpha\mathbf{q}'} \delta(\varepsilon - \varepsilon_{\mathbf{k}\alpha\sigma})$.

The lesser Green function $\mathcal{G}_a^<(\varepsilon)$ can be calculated by the Keldysh equation $\mathcal{G}_a^<(\varepsilon) = \mathcal{G}_a^r(\varepsilon)\Sigma^<(\varepsilon)\mathcal{G}_a^a(\varepsilon)$. To obtain $\Sigma^<(\varepsilon)$, we invoke Ng's ansatz³⁰: $\Sigma^<(\varepsilon) = \Sigma_0^<(\varepsilon)B$, where $\Sigma_0^<(\varepsilon) = i[\Gamma_L f_L(\varepsilon) + R\Gamma_R R^\dagger f_R(\varepsilon)]$ is the lesser self-energy of the clean graphene system with

$$R = \begin{pmatrix} \cos \frac{\theta}{2} & -\sin \frac{\theta}{2} \\ \sin \frac{\theta}{2} & \cos \frac{\theta}{2} \end{pmatrix}.$$

B is determined by the condition $B = (\Sigma_0^r(\varepsilon) - \Sigma_0^a(\varepsilon))^{-1}(\mathcal{G}_a^{a-1}(\varepsilon) - \mathcal{G}_a^{r-1}(\varepsilon))$ with $\Sigma_0^r(\varepsilon)$ ($\Sigma_0^a(\varepsilon)$) denoting the retarded (advanced) self-energy of the clean graphene system. Under these considerations, we finally obtain

$$I = \frac{e}{\hbar} \int \frac{d\varepsilon}{2\pi} Tr[\Gamma_L \mathcal{G}_a^r(\varepsilon) \overline{\Sigma}^< \mathcal{G}_a^a(\varepsilon)] [f_R(\varepsilon) - f_L(\varepsilon)], \quad (13)$$

where $\overline{\Sigma}^< = R\Gamma_R R^\dagger B$. The remaining task is to calculate the retarded Green's function $\mathcal{G}_a^r(\varepsilon)$.

By the equation of motion and then impurity average, we can derive

$$\mathcal{G}_a^r(\varepsilon) = \overline{g}_a^r(\varepsilon) [1 - \overline{g}_a^r(\varepsilon) \Sigma^r(\varepsilon)]^{-1}, \quad (14)$$

where $\overline{g}_a^{r,a}(\varepsilon) = \frac{1}{N} \sum_{\mathbf{q}} g_{\mathbf{q}a, \mathbf{q}a}^{r,a}(\varepsilon)$ and $\Sigma^r = n_i V_0^2 g_c - \frac{i}{2} [\Gamma_L(\varepsilon) + R\Gamma_R(\varepsilon)R^\dagger]$ with n_i the impurity density, $g_{\mathbf{q}a, \mathbf{q}a}^{r,a}(\varepsilon) = \frac{\varepsilon}{(\varepsilon \pm i\eta)^2 - |\phi(\mathbf{q})|^2}$, and

$$g_c = \begin{pmatrix} \frac{1}{\varepsilon - \varepsilon_\uparrow} & 0 \\ 0 & \frac{1}{\varepsilon - \varepsilon_\downarrow} \end{pmatrix}. \quad (15)$$

Introducing a cutoff k_c leads to

$$\overline{g}_a^r(\varepsilon) = -F_0(\varepsilon) - i\pi\rho_0(\varepsilon), \quad (16)$$

$$F_0(\varepsilon) = \frac{\varepsilon}{D^2} \ln \frac{|\varepsilon^2 - D^2|}{\varepsilon^2}, \quad \rho_0(\varepsilon) = \frac{|\varepsilon|}{D^2} \theta(D - |\varepsilon|) \quad (17)$$

with $D = v_F k_c$ denoting a high-energy cutoff of the graphene bandwidth. k_c is chosen as to guarantee the conservation of the total number of states in the Brillouin zone after the linearization of the spectrum around the K point, this is achieved following the Debye's prescription. We know from the selfenergy in Eq. (14) that introducing the impurities is behaving like changing the Fermi level with the impurity concentration. A similar effect, i.e. the Fermi level can be tuned from lying in the conduction band to the gap, is experimentally demonstrated by doping Ca in a topological insulator Bi_2Se_3 ³¹. The position of the impurity level is also important since a resonance is clearly seen also as shown below. In Eq.(13), we further set the symmetrical voltage division: $\mu_{L,R} = E_F \pm \frac{1}{2}eV$, and put $E_F = 0$ in the numerical calculations. The occupation of an impurity $\langle n_\sigma \rangle$ which appears in the spin-dependent energy of impurities should be treated in a self-consistent way via the relation

$$\langle n_\sigma \rangle = -\frac{1}{\pi} \int_{-\infty}^{+\infty} d\varepsilon f(\varepsilon) \text{Im} G_f^r(\varepsilon), \quad (18)$$

where

$$G_f^r(\varepsilon) = (1 - \overline{g}_a^r \Sigma_d^r) [g_c^{-1} - \overline{g}_a^r (n_i V_0^2 + g_c^{-1} \Sigma_d^r)]^{-1} \quad (19)$$

with $\Sigma_d^r(\varepsilon) = -\frac{i}{2} [\Gamma_L(\varepsilon) + R\Gamma_R(\varepsilon)R^\dagger]$. In terms of the result of Eq.(13), the TMR can be obtained according to the conventional definition

$$TMR = \frac{I(0) - I(\pi)}{I(0)}, \quad (20)$$

where $I(0, \pi)$ is the current flowing through the system in the parallel (antiparallel) configuration.

III. BI- AND TRI-LAYER GRAPHENE

Let us consider a bilayer (trilayer) graphene by adding a second (third) layer according to Bernal-type stacking order (ABA). The inter-layer hopping energy is denoted by t_p . By a straightforward generalization of the mono-layer case we obtain the retarded Green's function for the bilayer graphene as

$$\mathcal{G}_{2a}^r(\varepsilon) = \Lambda_2(\varepsilon) [1 - \Lambda_2(\varepsilon) \Sigma^r(\varepsilon)]^{-1}, \quad (21)$$

where

$$\Lambda_2(\varepsilon) = \frac{1}{N} \sum_{\mathbf{q}} \frac{-\varepsilon v_F^2 |\mathbf{q}|^2 + \varepsilon^3 - t_p^2 \varepsilon}{v_F^4 |\mathbf{q}|^4 - 2\varepsilon^2 v_F^2 |\mathbf{q}|^2 + \varepsilon^4 - t_p^2 \varepsilon^2}. \quad (22)$$

For trilayer graphene we find

$$\mathcal{G}_{3a}^r(\varepsilon) = \Lambda_3(\varepsilon) [1 - \Lambda_3(\varepsilon) \Sigma^r(\varepsilon)]^{-1}, \quad (23)$$

where

$$\Lambda_3(\varepsilon) = -\frac{1}{N} \sum_{\mathbf{q}} \frac{A_1 v_F^4 |\mathbf{q}|^4 + B_1 v_F^2 |\mathbf{q}|^2 + C_1}{v_F^6 |\mathbf{q}|^6 + B_2 v_F^4 |\mathbf{q}|^4 + C_2 v_F^2 |\mathbf{q}|^2 + D_2} \quad (24)$$

with

$$A_1 = \varepsilon, \quad B_1 = t_p^2 \varepsilon - 2\varepsilon^3,$$

$$C_1 = \varepsilon^5 - 2t_p^2 \varepsilon^3, \quad B_2 = -3\varepsilon^2, \quad C_2 = -2t_p^2 \varepsilon^2 + 3\varepsilon^4,$$

and

$$D_2 = -\varepsilon^6 + 2t_p^2 \varepsilon^4.$$

Substituting Eqs.(21) and (23) in Eq.(13), we obtain the electric current through the bi- and tri-layer graphene with impurity atoms, and also the TMR according to Eq.(20). The summation over \mathbf{q} in Eqs.(22) and (24) may be performed by taking the continuum limit with a cutoff D and expanding the integrand in terms of partial fractions. The final results have the explicit form

$$\begin{aligned} \Lambda_2(\varepsilon) = & -\frac{1}{D^2} \left\{ \frac{\text{sgn}(\varepsilon) t_p}{2} \ln \left| \frac{(D^2 - x_1) x_2}{(D^2 - x_2) x_1} \right| \right. \\ & \left. + \frac{\varepsilon}{2} \ln \left| \frac{(D^2 - x_1)(D^2 - x_2)}{x_1 x_2} \right| \right\} - i \frac{\pi}{D^2} \left\{ \frac{\text{sgn}(\varepsilon) t_p}{2} \right. \\ & \times [\text{sgn}(\frac{dx_1}{d\varepsilon}) \theta(0 < x_1 < D^2) \\ & - \text{sgn}(\frac{dx_2}{d\varepsilon}) \theta(0 < x_2 < D^2)] \\ & \left. + \frac{\varepsilon}{2} [\text{sgn}(\frac{dx_1}{d\varepsilon}) \theta(0 < x_1 < D^2) \right. \\ & \left. + \text{sgn}(\frac{dx_2}{d\varepsilon}) \theta(0 < x_2 < D^2)] \right\}, \quad (25) \end{aligned}$$

where $\theta(x)$ is the step function, and $x_{1,2} = \varepsilon^2 \pm t_p |\varepsilon|$. For $\Delta = (2B_2^3 - 9B_2C_2 + 27D_2)^2 + 4(-B_2^2 + 3C_2)^3 \geq 0$,

$$\begin{aligned} \Lambda_3(\varepsilon) = & -\frac{1}{D^2} \left\{ \left[A_1 + \frac{A_1(x_2+x_3)x_1 + B_1x_1 - A_1x_2x_3 + C_1}{(x_2-x_1)(x_3-x_1)} \right] \right. \\ & \times \ln \left| \frac{D^2-x_1}{x_1} \right| + \frac{A_1(x_2+x_3)+B_1}{\sqrt{x_2x_3-(x_2+x_3)^2/4}} \\ & \times \left(\arctan \frac{D^2-(x_2+x_3)/2}{\sqrt{x_2x_3-(x_2+x_3)^2/4}} \right. \\ & \left. + \arctan \frac{(x_2+x_3)/2}{\sqrt{x_2x_3-(x_2+x_3)^2/4}} \right) \\ & + \frac{A_1(x_2+x_3)x_1 + B_1x_1 - A_1x_2x_3 + C_1}{(x_2-x_1)(x_3-x_1)} \\ & \times \left[\frac{-1}{2} \ln \frac{D^2-(x_2+x_3)+x_2x_3}{x_2x_3} \right. \\ & \left. + \frac{(x_2+x_3)/2-x_1}{2\sqrt{x_2x_3-(x_2+x_3)^2/4}} \right. \\ & \times \left(\arctan \frac{D^2-(x_2+x_3)/2}{\sqrt{x_2x_3-(x_2+x_3)^2/4}} \right. \\ & \left. + \arctan \frac{(x_2+x_3)/2}{\sqrt{x_2x_3-(x_2+x_3)^2/4}} \right) \left. \right\} \\ & - \text{sgn} \left(\frac{dx_1}{d\varepsilon} \right) \theta(0 < x_1 < D^2) \frac{\pi V_f^2}{D^2} \\ & \times \left[A_1 + \frac{A_1(x_2+x_3)x_1 + B_1x_1 - A_1x_2x_3 + C_1}{(x_2-x_1)(x_3-x_1)} \right], \end{aligned} \quad (26)$$

where

$$\begin{aligned} x_1 = & -\frac{B_2}{3} + \frac{1}{2^{1/3}} \frac{1}{3} \left\{ -2B_2^3 + 9B_2C_2 - 27D_2 \right. \\ & \left. + \sqrt{(2B_2^3 - 9B_2C_2 + 27D_2)^2 + 4(-B_2^2 + 3C_2)^3} \right\}^{1/3} \\ & + \frac{1}{2^{1/3}} \frac{1}{3} \left\{ -2B_2^3 + 9B_2C_2 - 27D_2 \right. \\ & \left. - \sqrt{(2B_2^3 - 9B_2C_2 + 27D_2)^2 + 4(-B_2^2 + 3C_2)^3} \right\}^{1/3}, \quad (27) \\ x_{2,3} = & -\frac{B_2}{3} + \frac{-\frac{1}{2} - i\frac{\sqrt{3}}{2}}{3} \frac{1}{2^{1/3}} \left\{ -2B_2^3 + 9B_2C_2 - 27D_2 \right. \\ & \left. \pm \sqrt{(2B_2^3 - 9B_2C_2 + 27D_2)^2 + 4(-B_2^2 + 3C_2)^3} \right\}^{1/3} \\ & + \frac{-\frac{1}{2} + i\frac{\sqrt{3}}{2}}{3} \frac{1}{2^{1/3}} \left\{ -2B_2^3 + 9B_2C_2 - 27D_2 \right. \\ & \left. \mp \sqrt{(2B_2^3 - 9B_2C_2 + 27D_2)^2 + 4(-B_2^2 + 3C_2)^3} \right\}^{1/3}. \quad (28) \end{aligned}$$

For $\Delta < 0$,

$$\begin{aligned} \Lambda_3(\varepsilon) = & -\frac{1}{D^2} \left\{ \left[A_1 + \frac{A_1(x_2+x_3)+B_1}{(x_2-x_1)(x_3-x_1)} \right] \right. \\ & \times \ln \left| \frac{D^2-x_1}{x_1} \right| - \left[\frac{A_1(x_2+x_3)+B_1}{x_3-x_2} \right. \\ & \left. + \frac{A_1(x_2+x_3)+B_1}{(x_2-x_1)(x_3-x_2)} \right] \ln \left| \frac{D^2-x_2}{x_2} \right| \\ & + \left[\frac{A_1(x_2+x_3)+B_1}{x_3-x_2} \right. \\ & \left. + \frac{A_1(x_2+x_3)+B_1}{(x_2-x_1)(x_3-x_2)} \right] \\ & - \left[\frac{A_1(x_2+x_3)+B_1}{(x_2-x_1)(x_3-x_1)} \right. \\ & \left. + \frac{A_1(x_2+x_3)+B_1}{(x_2-x_1)(x_3-x_1)} \right] \\ & \times \ln \left| \frac{D^2-x_3}{x_3} \right| - i \frac{\pi V_f^2}{D^2} \left\{ \text{sgn} \left(\frac{dx_1}{d\varepsilon} \right) \theta(0 < x_1 < D^2) \right. \\ & \times \left[A_1 + \frac{A_1(x_2+x_3)+B_1}{(x_2-x_1)(x_3-x_1)} \right] \\ & - \text{sgn} \left(\frac{dx_2}{d\varepsilon} \right) \theta(0 < x_2 < D^2) \left[\frac{A_1(x_2+x_3)+B_1}{x_3-x_2} \right. \\ & \left. + \frac{A_1(x_2+x_3)+B_1}{(x_2-x_1)(x_3-x_2)} \right] \\ & + \text{sgn} \left(\frac{dx_3}{d\varepsilon} \right) \theta(0 < x_3 < D^2) \left[\frac{A_1(x_2+x_3)+B_1}{x_3-x_2} \right. \\ & \left. + \frac{A_1(x_2+x_3)+B_1}{(x_2-x_1)(x_3-x_2)} \right] \\ & \left. - \left[\frac{A_1(x_2+x_3)+B_1}{(x_2-x_1)(x_3-x_1)} \right] \right\}, \end{aligned} \quad (29)$$

where

$$\begin{aligned} x_1 = & -\frac{B_2}{3} + \frac{2\sqrt{B_2^2-3C_2}}{3} \cos\left(\frac{\arccos T}{3}\right), \\ x_2 = & -\frac{B_2}{3} + \frac{2\sqrt{B_2^2-3C_2}}{3} \cos\left(\frac{2\pi+\arccos T}{3}\right), \\ x_3 = & -\frac{B_2}{3} + \frac{2\sqrt{B_2^2-3C_2}}{3} \cos\left(\frac{4\pi+\arccos T}{3}\right), \\ T = & -\frac{2(B_2^2-3C_2)B_2-3(B_2C_2-9D_2)}{2(B_2^2-3C_2)^{3/2}}. \end{aligned} \quad (30)$$

To determine $\langle n_\sigma \rangle$, we need to calculate the impurity Green's function $G_{i=2,3;f}^{\sigma\sigma',r}(t-t') = -i\theta(t-t')\langle \{f_\sigma(t), f_{\sigma'}^\dagger(t')\} \rangle$ for the bilayer and trilayer graphene. Using the equation of motion method we find

$$G_{i,f}^r(\varepsilon) = (1 - \Lambda_i(\varepsilon)\Sigma_d^r)[g_c^{-1} - \Lambda_i(\varepsilon)(niV_0^2 + g_c^{-1}\Sigma_d^r)]^{-1}. \quad (31)$$

Substituting Eq.(31) in Eq.(18), we find $\langle n_\sigma \rangle$ self-consistently.

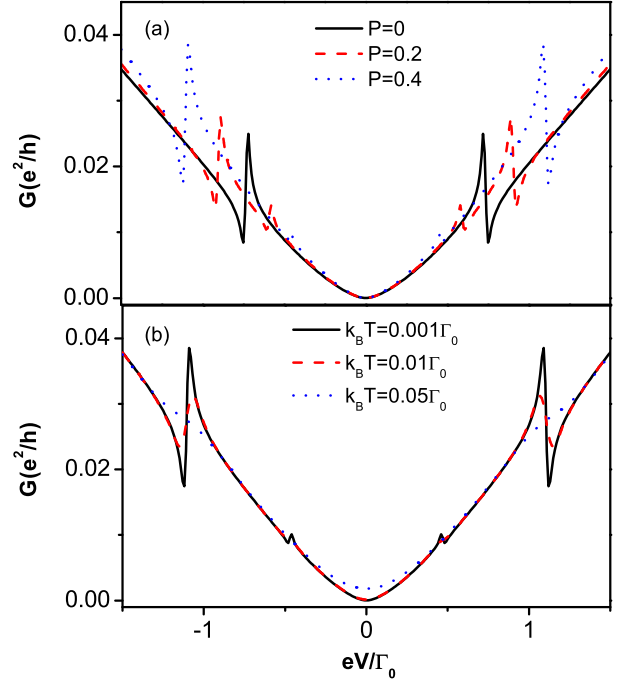


FIG. 2. (color online) The bias dependence of the differential conductance G for different polarizations P at $T = 0.001\Gamma_0$ (a) and for different temperatures T at $P = 0.4$ (b) for a single layer graphene junction and for parallel configuration of the electrodes magnetizations. The other parameters are taken as $V_f = 3\Gamma_0$, $n_i = 0.1$, $\varepsilon_0 = 0.1\Gamma_0$, $U = \Gamma_0$, $D = 5\Gamma_0$, where Γ_0 stands for the coupling between the scattering region and the electrodes.

IV. NUMERICAL ANALYSIS

To illustrate the nature of the spin-dependent transport we performed numerical calculations assuming the linewidth function $\Gamma_{\alpha}^{\sigma}(\varepsilon)$ to be independent of the energy within the wide band approximation. Introducing the degree of the spin polarizations of the left and the right electrodes, P_L and P_R , and assuming that the two electrodes are made of the same material, i.e. $P_L = P_R = P$, we can write $\Gamma_L^{\uparrow\downarrow} = \Gamma_R^{\uparrow\downarrow} = \Gamma_0(1 \pm P)$ where Γ_0 describes the coupling between the graphene and the electrodes in absence of an internal magnetization, and is taken as the energy scale in the following numerical calculation.

Fig.2(a) shows the bias dependence of the differential conductance $G = dI/dV$ in a single layer graphene system for the different P under the parallel configuration of the electrodes magnetizations. When $P = 0$ (nonmagnetic electrodes), the differential conductance possesses a single resonant peak as the bias voltage increases (or decreases) from zero up to few Γ_0 (or $-\Gamma_0$). This peak corresponds to a resonant tunneling through the renormalized spin-dependent impurity level $\varepsilon_0 + Un_{\sigma}$. Thereby, this situation reflects the fact that the impurity is not magnetized in the absence of the internal magnetization of the electrodes, i.e. $n_{\uparrow} = n_{\downarrow}$. When $P \neq 0$, the aforementioned single peak in the conductance splits into two peaks indicating the positions of the resonant tunneling at $\varepsilon_0 + Un_{\uparrow}$ and $\varepsilon_0 + Un_{\downarrow}$ and signaling the form of the localized magnetic moment of the impurity. This behavior is due to the fact that the exchange splitting of the density of state (DOS) in the ferromagnetic leads acts as an effective magnetic field with values well larger than those of an externally applied field^{32,33}. This effective field acts on the graphene including the impurity atoms and influences strongly the spin states of the impurities. With increasing P the peaks split further way from each other signifying that the polarization in the ferromagnetic leads enhances the localized magnetic moment. With increasing P , the peak at the higher voltage is enhanced and that at the lower voltage is suppressed. This non-monotonic dependence of the peak amplitude on the polarization of the electrodes is completely different from the ferromagnet-quantum dot-ferromagnet(FM-QD-FM) system³⁴⁻³⁶; its origin stems from the linear DOS of graphene. The dependence of the differential conductance on the bias for different temperatures in a parallel configuration is shown in Fig. 2(b) for a single layer graphene device. With increasing the temperature, the resonant peaks in the differential conductance decrease and almost vanish at larger T . This temperature dependence of the conductance peaks is similar to that of a noninteracting, single-particle resonance in the multi-channel model. The mechanism for this destruction of the peak is that at high temperatures not all electron states of the low-lying subbands are fully occupied due to the occupation of the next subbands³⁷. However, near $V = 0$, the conductance increases when the temperature is raised. This characteristic feature is the same as

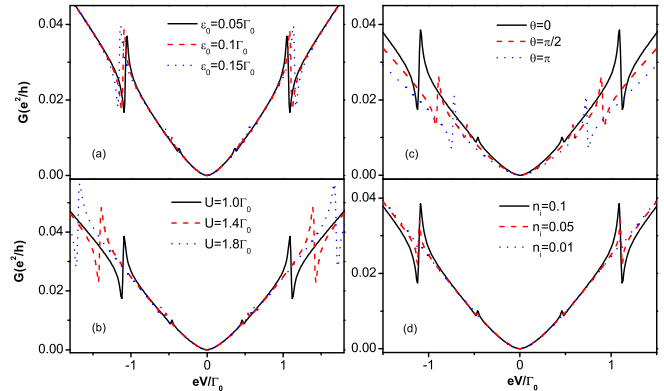


FIG. 3. (color online) The bias dependence of the differential conductance G for different energies ε_0 of the impurity level at $U = \Gamma_0$, $\theta = 0$ and $n_i = 0.1$ (a), for different interaction strengths U at $\varepsilon_0 = 0.1\Gamma_0$, $\theta = 0$ and $n_i = 0.1$ (b), and for different angles θ at $\varepsilon_0 = 0.1\Gamma_0$, $U = \Gamma_0$ and $n_i = 0.1$ (c) as well as for the different impurity concentrations n_i at $\varepsilon_0 = 0.1\Gamma_0$, $U = \Gamma_0$ and $\theta = 0$ (d). A single layer of graphene is considered. The other parameters are taken the same as those of Fig.2.

that in the clean undoped graphene systems¹⁰. The reason is the graphene acts as a barrier at the zero energy point. Near zero-bias voltage, the increase of the thermally excited electrons with the temperature enhances the conductance.

The bias dependence of the differential conductance of a single layer graphene device for different ε_0 and different interaction U is shown in Fig. 3(a) and (b). With increasing ε_0 and U , the resonant peaks in the conductance shift towards large bias voltages, and the peaks amplitudes become large which is also related to the linear DOS of the graphene. In particular, one can find that the interval between the conductance peaks increases with the interaction U , in contrast it decreases with ε_0 . This is because the DOS around the impurity energy level is enhanced as ε_0 grows, which decreases the localized magnetic moment on the impurity^{16,18}. Fig.3(c) shows for a single layer graphene tunnel junction the bias dependence of the differential conductance when varying the mutual angle θ between the electrodes magnetization direction. With increasing θ , the split structure of the resonant peaks in the differential conductance is washed out, and eventually the two peaks merge into a single peak at $\theta = \pi$, meaning that the impurity loses its magnetism in this situation. This behavior suggests that the magnetization electrodes can be used as a valve device to open or close the magnetism of impurity atoms in graphene. Similar phenomena has also been observed in the FM-QD-FM system^{32,38}, where the magnetic moment in the quantum dot is induced by different spin-dependent tunneling rates between the two magnetic electrodes. In our

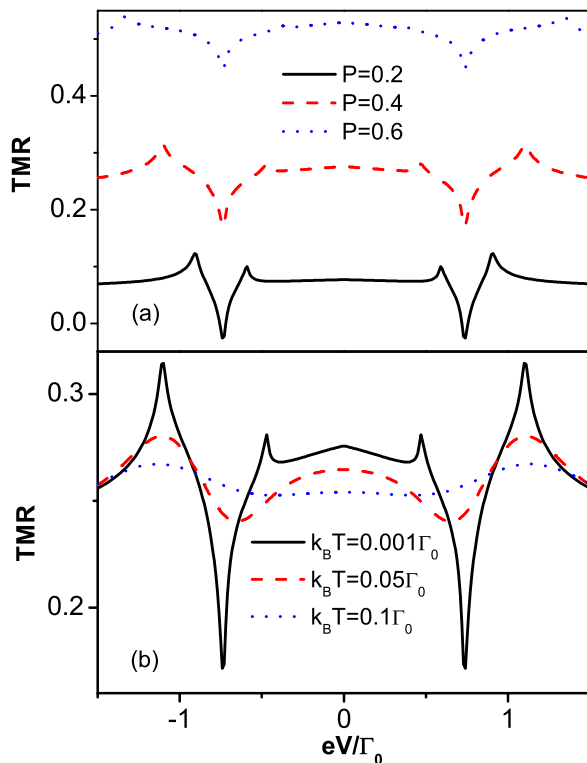


FIG. 4. (color online) The bias dependence of the TMR for different degrees of polarization P at $T = 0.001\Gamma_0$ (a) and for different temperatures T at $P = 0.4$ (b) for a single layer graphene tunnel junction. The other parameters are taken the same as those of Fig.2.

case, the impurity atom immerses in the Dirac fermions sea. Its magnetic moment is turned on via a mediation of the itinerant massless Dirac fermion not via a direct tunneling^{16,18}. This shows new features as discussed above and below. In Fig. 3(d), we plot the differential conductance as a function of bias voltage for different impurity concentrations in a single layer graphene device. One can easily observe that the resonant peaks diminish with decreasing the impurity concentration, however their positions do not change. This suggests that the magnetization is maintained although with descendent effect of the impurities on transport in graphene at lower concentration since the information of the magnetizations of the electrodes is transmitted by the Dirac fermions in the same way.

The bias dependence of the TMR, defined in Eq.(20), for different polarizations P and the different temperatures T in a single layer graphene junction is shown in Fig.4. A small hump at zero bias corresponds to an enhanced magnetoresistance due to the result of a nontrivial combined effect of graphene and conventional spin-

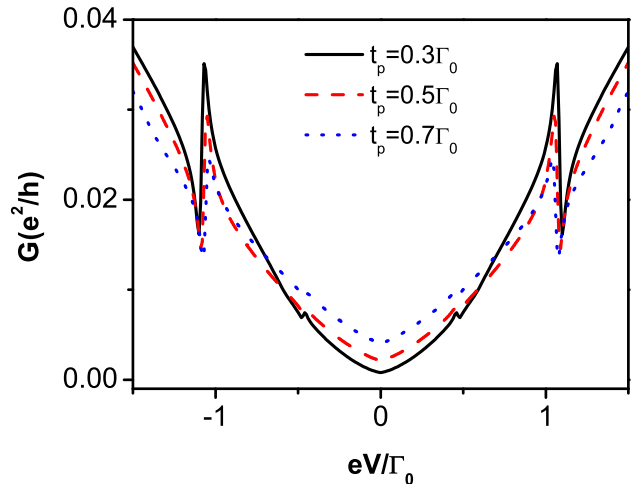


FIG. 5. (color online) The bias dependence of the differential conductance G for different interlayer couplings t_p at $T = 0.001\Gamma_0$ and $P = 0.4$ for the bilayer graphene system. The other parameters are taken the same as those of Fig.2.

valve properties¹⁰. The existence of the impurity suppresses the amplitude of this structure since the impurity influence on the DOS extends to the Dirac point³⁹. Additionally, it is found that the TMR as a function of the bias voltage exhibits two pronounced dips at lower and higher bias. The latter one is particularly interesting as the TMR there may change sign from positive to negative for small values of the polarization parameters. To account for this behavior one should take into account the angular dependence of the conductance from Fig.3(c) which shows clearly the change of the positions and the heights of the peak with the angle θ , leading to the appearance of the negative TMR. For large bias (see Fig. 4(b)), the graphene system with the impurity atoms behaves like that in the absence of the impurities¹⁰, where TMR hardly changes with temperature T . This phenomena suggests that the presence of the impurity atoms does not affect the magnetoresistance at high bias voltages. However, for a low bias voltage, TMR displays many important features: With increasing temperatures the hump at zero bias diminishes since the increase in the electrical current from the contribution of thermally excited electrons is faster for the antiparallel configuration. Additionally, the dip in TMR decreases with T . Therefore, due to their combinations, TMR near the zero bias voltage displays a broad peak instead of the "W"-shape feature with increasing the temperature T , and eventually develops into a broad dip.

Fig.5 shows the bias dependence of the differential conductance in a bilayer graphene system. When the interlayer coupling grows, the conductance at zero bias increases, while the resonant peak diminishes. The ex-

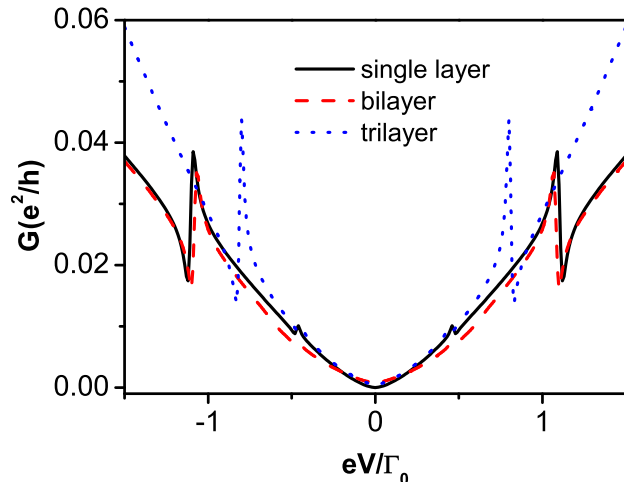


FIG. 6. (color online) The bias dependence of the differential conductance G for different layer graphene at $T = 0.001\Gamma_0$, $P = 0.4$ and $t_p = 0.3\Gamma_0$. The other parameters are taken the same as those of Fig.2.

planation for this phenomenon is as follows: the quasi-particles in the bilayer graphene have a peculiar nature with features akin both to Dirac and to conventional fermions. The contribution of conventional fermions originates from the interlayer coupling that supports a metallic bilayer graphene. Thus the increase of the interlayer coupling enhances the zero bias conductance in the bilayer graphene. Furthermore, the metallic behavior due to the interlayer coupling enhances the screening of the impurity^{40,41}, which leads to the decrease of the transmission probability of the electrons, thus suppressing the resonant tunneling through the energy level $\varepsilon_0 + n_\sigma U$. The bias dependence of the differential conductance for the different layer graphene devices is shown in Fig. 6. The differential conductance for all the graphene layers displays two peaks corresponding to the resonant tunneling through the energy level $\varepsilon_0 + n_\sigma U$. It is suggested that the impurity magnetic moment also exists for the bi-

layer and trilayer graphene when the ferromagnetic electrodes are introduced. However, the distance of the two peaks decreases with increasing the number of graphene layers. This result stems from the fact that the impurity magnetic moment decreases with increasing the layer number¹⁸.

V. SUMMARY

In conclusion, using Keldysh's nonequilibrium Green's function method, we study theoretically the spin dependent transport through a tunnel junction made of few layers of graphene with impurity atoms. It is found that when the electrodes magnetization vectors are parallel, the bias dependence of the differential conductance exhibits two resonant peaks as the bias voltage increases. We assign this behavior to the formation of a magnetic moment on the impurity due to the electrodes spin polarization. With increasing the mutual angle θ between the vectors of the two electrodes magnetization, the distance of the two resonant peaks in the differential conductance diminishes, and they merge eventually into a single peak at $\theta = \pi$. The reason is that the induced magnetic moment on the impurity decreases with θ and vanishes for $\theta = \pi$. This features may be exploited to develop a magnetic valve device that operates based on the presence or the absence of the magnetism on the impurity atom. Furthermore, due to the θ -dependence of the impurity magnetic moment, the TMR may change sign for small values of the polarization parameters.

ACKNOWLEDGMENTS

The work of K.H.D. and Z.H.Z. was supported by the National Natural Science Foundation of China (Grant Nos. 10904007 and 60771059), the Natural Science Foundation of Hunan Province, China (Grant No. 08JJ4002), and the construct program of the key discipline in Changsha University of Science and Technology, China. J.B. and Z.G.Z. were supported by the cluster of excellence "Nanostructured Materials" of the state Saxony-Anhalt, and the DFG, Germany.

¹ K. S. Novoselov, A. K. Geim, S. V. Morozov, D. Jiang, M. I. Katsnelson, I. V. Grigorieva, S. V. Dubonos, and A. A. Firsov, *Nature* **438**, 197 (2005).

² Y. Zhang, Y. W. Tan, H. L. Stormer, and P. Kim, *Nature* **438**, 201 (2005).

³ A. K. Geim and K. S. Novoselov, *Nature Materials* **6**, 183 (2007).

⁴ A. H. Castro Neto, F. Guinea, N. M. R. Peres, K. S. Novoselov, A. K. Geim, *Rev. Mod. Phys.* **81**, 109 (2009).

⁵ E. W. Hill, A. K. Geim, K. Novoselov, F. Schedin, and P. Black, *IEEE Trans. Magn.* **42**, 2694 (2006).

⁶ N. Tombros, C. Jozsa, M. Popinciuc, H. T. Jonkman, and B. J. Van Wees, *Nature* **448**, 571 (2007).

⁷ S. Cho, Yung-Fu Chen, and M. S. Fuhrer, *Appl. Phys. Lett.* **91**, 123105 (2007).

⁸ M. Ohishi, M. Shiraishi, R. Nouchi, T. Nozaki, T. Shinjo, and Y. Suzuki, *Jpn. J. Appl. Phys.* **46**, L605 (2007).

⁹ W. H. Wang, K. Pi, Y. Li, Y. F. Chiang, P. Wei, J. Shi, and R. K. Kawakami, *Phys. Rev. B* **77**, 020402(R) (2008).

¹⁰ K.H. Ding, Z.G. Zhu, and J. Berakdar, *Phys. Rev. B* **79**, 045405 (2009).

¹¹ S.Krompiewski, *Phys. Rev. B* **80**, 075433 (2009).

- ¹² K.H. Ding, Z.G. Zhu, and J. Berakdar *Europhysics Letters* **88**, 58001 (2009)
- ¹³ J.C. Chen *et al.*, *J. Phys.:Condens. Matter* **22**, 035301 (2010)
- ¹⁴ K.-H. Ding, G. Zhou, Z.-G. Zhu, J. Berakdar, *J. Phys.: Condens. Matter* **20**, pp 345228 (2008).
- ¹⁵ J.C. Meyer *et al.*, *Nature* **454**, 319 (2008).
- ¹⁶ B. Uchoa, V. N. Kotov, N. M. R. Peres, and A. H. Castro Neto, *Phys. Rev. Lett.* **101**, 026805 (2008).
- ¹⁷ A. H. Castro Neto, Valeri N. Kotov, Johan Nilsson, Vitor M. Pereira, Nuno M. R. Peres, Bruno Uchoa, *Sol. Stat. Comm.* **149**, 1094 (2009).
- ¹⁸ K.-H. Ding, Z.-G. Zhu, J. Berakdar, *J. Phys.: Condens. Matter* **21**, 182002 (2009).
- ¹⁹ B. Uchoa, L. Yang, S.-W. Tsai, N. M. R. Peres, A. H. Castro Neto, *Phys.Rev. Lett.* **103**, 206804 (2009).
- ²⁰ M. Hentschel and F. Guinea, *Phys. Rev. B* **76**, 115407 (2007).
- ²¹ B. Dóra and P. Thalmeier, *Phys. Rev. B* **76**, 115435 (2007).
- ²² P. S. Cornaglia, G. Usaj, and C. A. Balseiro, *Phys. Rev. Lett.* **102**, 046801 (2009).
- ²³ H. B. Zhuang, Q. F. Sun, and X. C. Xie, *Eur. Phys. Lett.* **86**, 58004 (2009).
- ²⁴ Z. G. Zhu, K. H. Ding, and J. Berakdar, *Europhys. Lett.* **90**, 67001 (2010).
- ²⁵ T. O. Wehling, H. P. Dahal, A. I. Lichtenstein, M. I. Katsnelson, H. Manoharan, and A. V. Balatsky, arXiv:0906.2426.
- ²⁶ H. Haug and A. P. Jauho, *quantum kinetics in transport and optics of semiconductors* (Springer, Berlin, 1998).
- ²⁷ J. Rammer, *quantum transport theory* (Westview Press, 2004).
- ²⁸ N. A. Sinitsyn, J. E. Hill, H. Min, J. Sinova, and A. H. MacDonald, *Phys. Rev. Lett.* **97**, 106804 (2006)
- ²⁹ T. S. Nunner, N. A. Sinitsyn, Mario F. Borunda, V. K. Dugaev, A. A. Kovalev, Ar. Abanov, C. Timm, T. Jungwirth, J. Inoue, A. H. MacDonald, and J. Sinova, *Phys. Rev. B* **76**, 235312 (2007).
- ³⁰ T. K. Ng, *Phys. Rev. Lett.* **76**, 487 (1996).
- ³¹ J. G. Checkelsky, Y. S. Hor, M.-H. Liu, D.-X. Qu, R. J. Cava, and N. P. Ong, *Phys. Rev. Lett.* **103**, 246601 (2009).
- ³² A.N. Pasupathy, et al., *Science* **306**, 86 (2004).
- ³³ Z. G. Zhu, *Phys. Lett. A* **372**, 695 (2008).
- ³⁴ N. Sergueev, Q.-F. Sun, H. Guo, B. G. Wang, and J. Wang, *Phys. Rev. B* **65**, 165303 (2002).
- ³⁵ H.-F. Mu, G. Su, and Q.-R. Zheng, *Phys. Rev. B* **73**, 054414 (2006).
- ³⁶ Z.-G. Zhu, G. Su, Q.-R. Zheng, and B. Jin, *Phys. Rev. B* **70**, 174403 (2004).
- ³⁷ B.J. van Wees, L.P. Kouwenhoven, E.M.M. Willems, C.J.P.M. Harmans, J.E. Mooij, H. van Houten, C.W.J. Beenakker, J.G. Williamson, C.T. Foxon, *Phys. Rev. B* **43**, 12431 (1991).
- ³⁸ P. Zhang, Q. K. Xue, and X. C. Xie, arXiv:cond-mat/0201465.
- ³⁹ J. Nilsson and A. H. Castro Neto, *Phys. Rev. Lett.* **98**, 126801 (2007).
- ⁴⁰ D. P. DiVincenzo and E. J. Mele, *Phys. Rev. B* **29**, 1685 (1984).
- ⁴¹ N. M. R. Peres, F. Guinea, and A. H. Castro Neto, *Phys. Rev. B* **73**, 125411(2006).